STRESS-SINGULARITY AND GENERALIZED FRACTURE TOUGHNESS AT THE VERTEX OF RE-ENTRANT CORNERS

ALBERTO CARPINTERI
Istituto di Scienza delle Costruzioni, Università di Bologna, Viale Risorgimento 2, 40136 Bologna, Italy

Abstract—The object of the present paper is the definition of the size scale effects in structural members with re-entrant corners. The interaction between stress-intensity collapse and ultimate strength collapse at the ligament is emphasized. Such interaction is considerable for small sizes and large corner angles. The results of an experimental analysis on PMMA notched beams are reported and discussed. When the re-entrant corner angle is close to 180° the stress-singularity tends to disappear and the generalized stress-intensity factor assumes the physical dimensions of stress, $[F][L]^{-2}$. On the other hand, when the re-entrant corner angle is close to 0° the stress-singularity tends to the well-known LEFM value 1/2 so that the stress-intensity factor assumes the classical dimensions $[F][L]^{-3/2}$. The experimental evaluation of the shape-function for generalized stress-intensity factors is carried out on statistical bases by assuming non-linear combinations of LEFM function and ultimate strength function. Due to the accidentally very similar aspect of the two functions, the experimental evaluation of generalized fracture toughness results in particular difficulty.

1. INTRODUCTION

SINCE THE pioneer paper by Williams[1] the problem of stress intensification at the vertex of re-entrant corners has been disregarded if compared with its considerable practical importance. It is much more frequent to know shape and size of notches or re-entrant corners in structural components than shape and size of cracks. In spite of this, fracture mechanics applied to sharp cracks has been broadly developed in the last two decades, even if it is only a particular case[2] of the more general problem of re-entrant corners.

Very notable is the investigation on stress intensification at the vertex of re-entrant corners carried out at CSIRO Australian Forest Production Laboratory, Division of Building Research. Leicester[3] emphasized the size scale effects in structures with re-entrant corners due to the presence of a stress-singularity and noted that they may not occur unless member sizes are sufficiently large. Consequently such scale effects may not appear in scaled-down laboratory testing. The work by Leicester was continued by Walsh[4] extending conventional finite element procedures to non-zero angle notch problems. He considered also the problem of crack initiation at corners of openings in walls and examined the effect of beam size on the sharp crack propagation in concrete[5].

More recently, Sinclair and Kondo[6] considered the determination of realistic measures for the peak local stresses occurring at sharp re-entrant corners in plates under remote transverse loading. They gave up the singular character of re-entrant corners and carried out experimental investigation on classical stress concentration. Then, the Reciprocal Work Contour Integral Method was used by Carpenter[7] to obtain the stress singularity at the tip of corner configurations. In this way, he performed the numerical analysis of a lap joint with 90° corner angles in mixed mode loading.

The object of the present paper is to define the size scale effects in structural members with re-entrant corners and to emphasize the interaction between stress-intensity collapse and ultimate strength collapse at the ligament. Such interaction is considerable for small sizes[8, 9] and large corner angles. A similar stress-singularity attenuation and collapse transition was pointed out by Carpinteri[10] for strain-hardening Ramberg–Osgood materials.

The results of an experimental analysis on PMMA notched beams are reported and discussed. When the re-entrant corner angle is close to 180°, the stress-singularity tends to disappear and the generalized stress-intensity factor assumes the physical dimensions of stress, $[F][L]^{-2}$. On the other hand, when the re-entrant corner angle is close to 0°, the stress-singularity tends to the well-known LEFM value 1/2 so that the stress-intensity factor assumes the classical dimensions $[F][L]^{-3/2}$.

The experimental evaluation of the shape-function for generalized stress-intensity factors is carried out on statistical bases by assuming non-linear combinations of LEFM function and ultimate

strength function. Due to the very similar aspect of such two functions, the experimental evaluation of critical generalized stress-intensity factors results to be particularly difficult.

2. SIZE SCALE EFFECTS IN STRUCTURES WITH RE-ENTRANT CORNERS

Let us consider a two-dimensional linear elastic structure with an edge sharp crack (Fig. 1a). The symmetrical stress field around the crack tip can be described by the following expression:

$$\sigma_{ij} = K_1 r^{-1/2} S_{ij}(\varphi), \tag{1}$$

where K_1 is the stress-intensity factor and r, φ are the radial and angular coordinates respectively.

For every geometrical shape of the structure, it is possible to express the K_1-factor as:

$$K_1 = \sigma b^{1/2} f(a/b), \tag{2}$$

where σ is the nominal stress, b is a characteristic size of the structure, f is a shape-function depending on the geometry of structure and on the ratio of crack length a to reference size b. The stress of failure

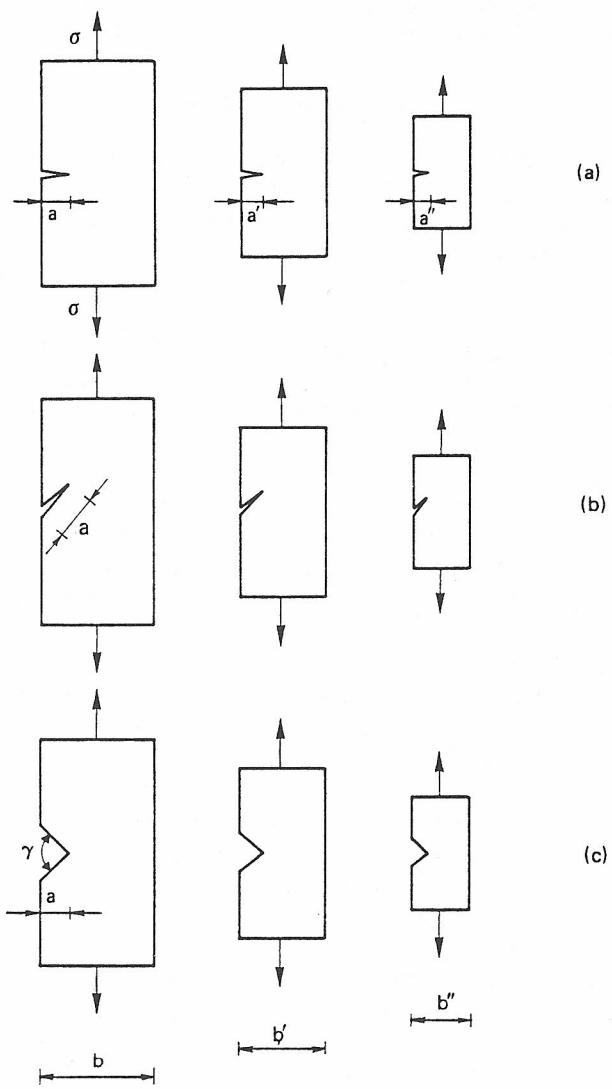

Fig. 1. Geometrically similar structures with one defect: (a) opening crack, (b) mixed mode crack, (c) re-entrant corner.

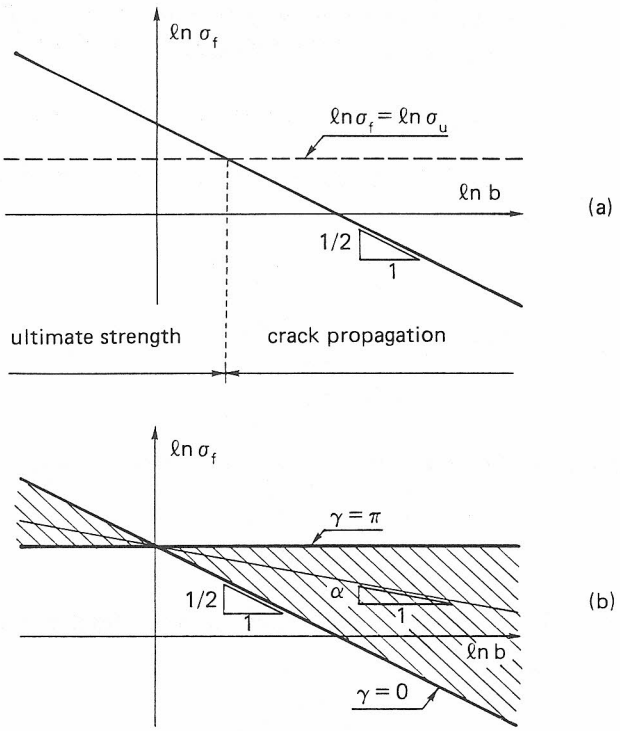

Fig. 2. Bi-logarithmic strength vs size diagram: (a) interaction between ultimate strength collapse and crack propagation, (b) attenuation of the strength decrease when the re-entrant corner angle increases.

σ_f is achieved when the K_1-factor is equal to its critical value K_{1C}:

$$\sigma_f = K_{1C} b^{-1/2} \frac{1}{f(a/b)}. \tag{3}$$

If the logarithms of both members of eq. (3) are considered, we obtain:

$$\ln \sigma_f = [\ln K_{1C} - \ln f(a/b)] - \tfrac{1}{2} \ln b, \tag{4}$$

or, more synthetically:

$$\ln \sigma_f = A\left(K_{1C}, \frac{a}{b}\right) - \frac{1}{2} \ln b, \tag{5}$$

where function A depends on the shape of structure, besides on material and crack depth.

If we keep material and structural shape constant and take into consideration a set of geometrically similar structures (Fig. 1a), the strength $\ln \sigma_f$ will result in a linear decreasing function with negative slope 1/2 of the scale-parameter $\ln b$ (Fig. 2a). If the material presents an intrinsic strength σ_u, the horizontal line:

$$\ln \sigma_f = \ln \sigma_u, \tag{6}$$

will bound the strength for $b \to 0$ in the diagram of Fig. 2a. In fact, as observed by the writer[8, 9], when the structural size is relatively small, the ultimate strength collapse precedes crack propagation.

When the sharp crack is subjected to a mixed mode loading condition (Fig. 1b), the stress field at the crack tip is:

$$\sigma_{ij} = \sum_{m=1}^{2} K_m r^{-1/2} S_{ij}^{(m)}(\varphi), \tag{7}$$

where K_m ($m = 1, 2$) are the stress-intensity factors related to mode 1 (opening) and mode 2 (sliding) respectively. Analogously to eq. (2), they can be expressed as:

$$K_m = \sigma b^{1/2} f_m(a/b); \qquad m = 1, 2. \tag{8}$$

The interaction of the two fundamental fracture modes produces crack propagation when a function of K_m ($m = 1, 2$) is equal to its critical value:

$$F(K_m; m = 1, 2) = F_c. \tag{9}$$

Most relevant fracture criteria can be approximated by an elliptic function F[12]:

$$K_1^2 + qK_2^2 = K_{1C}^2, \tag{10}$$

where q ($\geqslant 0$) is a measure of the influence of mode 2 on crack propagation. Recalling eq. (8) it follows:

$$\sigma^2 b(f_1^2 + qf_2^2) = K_{1C}^2, \tag{11}$$

and, therefore, the stress of failure is given by eq. (3) again, with function f replaced by the square root:

$$f = \sqrt{f_1^2 + qf_2^2}. \tag{12}$$

Thus, even in the case of mixed mode crack, the scale effect is represented by a straight line with negative slope 1/2 in the plane $\ln \sigma_f$–$\ln b$ (Fig. 2a). This means that it is the power of the stress-singularity, and not the geometry of crack, structure and load, which determines the rate of strength decrease by increasing the size scale.

Let us consider now a two-dimensional linear elastic structure with a re-entrant corner of amplitude γ (Fig. 1c). Williams[1] proved that when both notch surfaces are free, the symmetrical stress field at the notch tip is:

$$\sigma_{ij} = K_1^* r^{-\alpha} S_{ij}^{(\gamma)}(\varphi), \tag{13}$$

where the power α of the stress-singularity is provided by the eigen-equation:

$$(1-\alpha)\sin(2\pi-\gamma) = \sin[(1-\alpha)(2\pi-\gamma)], \tag{14}$$

and ranges between 1/2 (when $\gamma = 0$) and zero (when $\gamma = \pi$), as is illustrated by the diagram in Fig. 3. If Buckingham's theorem for physical similitude and scale modelling is applied and stress and linear size are assumed as fundamental quantities[8], it is possible to write an equation analogous to eq. (2):

$$K_1^* = \sigma b^{\alpha} f^*(a/b). \tag{15}$$

When angle γ vanishes, eq. (15) coincides with eq. (2), whereas when $\gamma = \pi$ the stress-singularity disappears and the generalized stress-intensity factor K_1^* assumes the physical dimensions of stress and becomes proportional to the nominal stress σ. As experimentally demonstrated by Leicester[3], the stress of failure σ_f is achieved when the K_1^* factor is equal to its critical value K_{1C}^*:

$$\sigma_f = K_{1C}^* b^{-\alpha} \frac{1}{f^*(a/b)}, \tag{16}$$

and in logarithmic form:

$$\ln \sigma_f = B(K_{1C}^*, a/b) - \alpha \ln b, \tag{17}$$

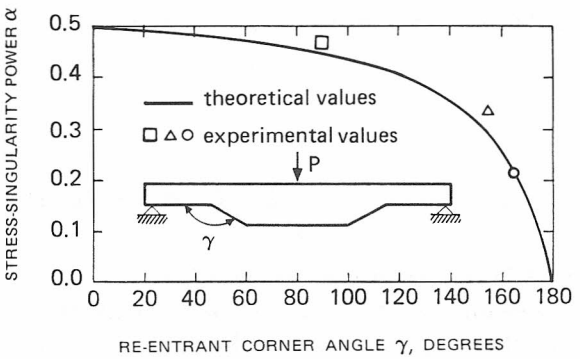

Fig. 3. Stress-singularity power vs re-entrant corner angle.

where:

$$B(K_{1C}^*, a/b) = \ln K_{1C}^* - \ln f^*(a/b). \tag{18}$$

If we keep material and structural shape constant and take into consideration a set of geometrically similar structures (Fig. 1c), the strength $\ln \sigma_f$ results in a linear decreasing function with negative slope α of the scale-parameter $\ln b$ (Fig. 2b). When $\gamma \to \pi$, i.e. when $\alpha \to 0$, any scale effect vanishes and the straight line becomes horizontal. In this case the equilibrium condition is:

$$\sigma b = K_1^*(b-a), \tag{19}$$

and then, from eq. (15):

$$f^*(a/b) = \frac{1}{1-(a/b)}. \tag{20}$$

When the notch depth a/b tends to zero, the shape-function is $f^*(a/b) = 1$ and the generalized stress-intensity factor K_1^* coincides with the nominal stress σ exactly, see eq. (15). The distinction between ultimate strength collapse and fracture at the corner tip vanishes and condition (17) coincides with condition (6).

The case of re-entrant corner subjected to mixed mode loading can be handled in the same way as was done for the sharp crack. Even in this case the conclusion is that only the power of the stress-singularity determines the rate of decrease in strength with size and not the loading condition.

Some experimental confirmations of what has been said are presented in Fig. 4. Leicester[3] tested geometrically similar timber beams with re-entrant corners and found very clear size effects of

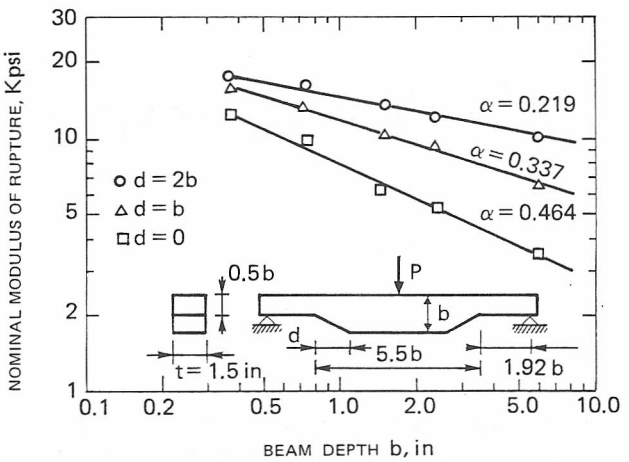

Fig. 4. Effect of size on bending strength of timber beams with re-entrant corners.

the type described above. The rate of strength decrease coincides with that predicted by the theory (Fig. 3).

3. EXPERIMENTAL EVALUATION OF THE SHAPE-FUNCTION FOR RE-ENTRANT CORNERS

The shape-function f^* in eq. (15) is generally not known as well as the critical value of the generalized stress-intensity factor K^*_{1C}. An experimental investigation was then carried out by the writer in order to define a practical procedure to find such a parameter. Three-point bending tests were performed on PMMA notched beams of span $l = 19$ cm, depth $b = 5$ cm and thickness $t = 5$ cm. Two different notch depths, $a = 1, 2$ cm, and six different re-entrant corner angles, $\gamma = 0°, 45°, 90°, 120°, 150°, 180°$, were selected (Fig. 5). The two extreme cases, $\gamma = 0°$ and $\gamma = 180°$, were realized with narrow sawed slits 0.5 mm thick and with unnotched specimens of reduced cross-section ($b = 3, 4$ cm) respectively. Three identical specimens were considered for each one of the 12 cases contemplated with a total number of 36 specimens.

The values of failure load are reported for each single specimen in Tables 1 and 2, related to $a = 1$ cm and $a = 2$ cm respectively. Even the average values and their ratios to the unnotched specimen values are shown. The latter are represented in Fig. 6 vs the re-entrant corner angle. The relative strength increase is far from being linear, with a nearly constant value up to about 90° and then a sharp variation to achieve the unit value for $\gamma = 180°$. Such function is nearly independent of the relative crack depth a/b. This implies that the shape-function f^* of the generalized stress-intensity factor:

$$K_1^* = \frac{Pl}{tb^{(2-\alpha)}} f^*\left(\frac{a}{b}, \gamma\right), \tag{21}$$

should obey the proportionality relation:

$$f^*\left(\frac{a}{b}, \gamma\right) \simeq C(\gamma) g\left(\frac{a}{b}\right). \tag{22}$$

Function f^* is then separable into two functions, each one with a single argument.

The previous experimental result is not surprising if the extreme shape-functions f and g, related to sharp cracks ($\gamma = 0°$) and vanishing (or flat) re-entrant corner angles ($\gamma = 180°$) respectively, are considered:

$$K_1^*(\gamma = 0°) = K_1 = \frac{Pl}{tb^{3/2}} f\left(\frac{a}{b}\right), \tag{23a}$$

with[11]

$$f\left(\frac{a}{b}\right) = 2.9\left(\frac{a}{b}\right)^{1/2} - 4.6\left(\frac{a}{b}\right)^{3/2} + 21.8\left(\frac{a}{b}\right)^{5/2} - 37.6\left(\frac{a}{b}\right)^{7/2} + 38.7\left(\frac{a}{b}\right)^{9/2}, \tag{23b}$$

and

$$K_1^*(\gamma = 180°) = \sigma = \frac{Pl}{tb^2} g\left(\frac{a}{b}\right), \tag{24a}$$

with

$$g\left(\frac{a}{b}\right) = \frac{1.5}{(1 - a/b)^2}. \tag{24b}$$

The shape-functions f and g are represented in Fig. 7 and they both appear strongly varying with the relative notch depth a/b, but their ratio is nearly constant for $0.1 \lesssim a/b \lesssim 0.5$.

Function $C(\gamma)$ in eq. (22) presents the two extreme values: $C(0) \simeq 1/2$ and $C(\pi) = 1$, and its non-

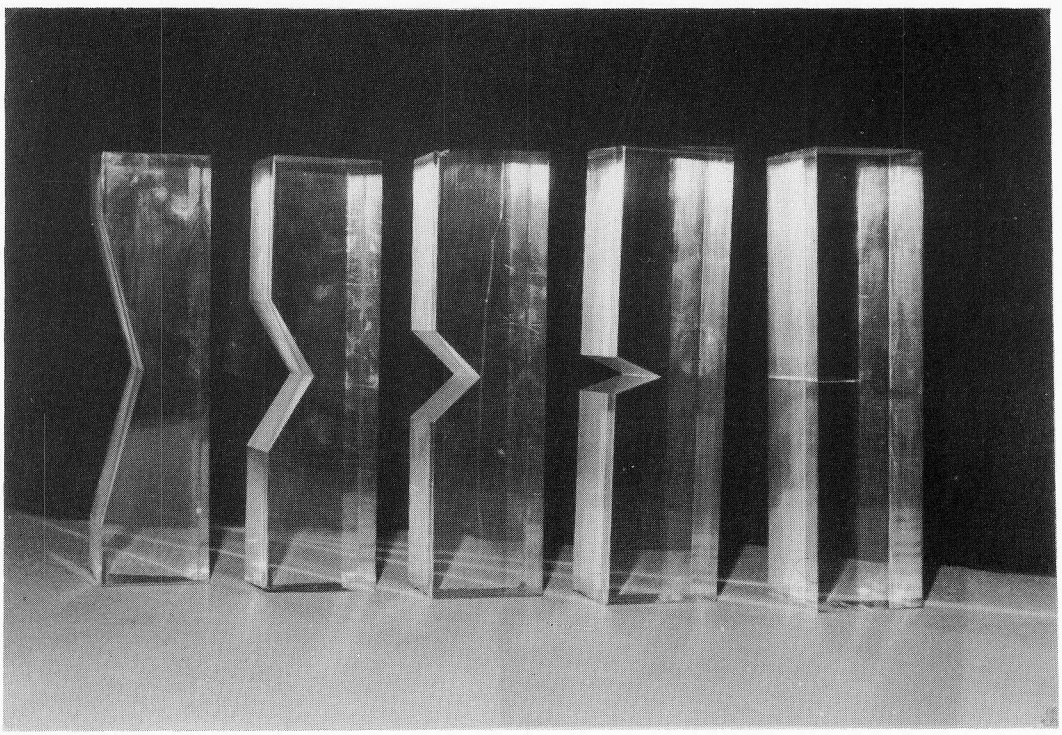

Fig. 5. PMMA beams with re-entrant corners used in the experimental investigation carried out by the author.

Table 1. Failure loads (notch depth: $a = 1$ cm)

Angle γ	I	II	III	Average value	$P_{CR}(\gamma)/P_{CR}(180°)$
0°	462	474	552	496	0.13
45°	470	460	465	465	0.12
90°	582	618	587	596	0.16
120°	745	760	675	727	0.19
150°	1225	1070	870	1055	0.28
180°	3770	3780	3930	3827	1.00

Table 2. Failure loads (notch depth: $a = 2$ cm)

Angle γ	I	II	III	Average value	$P_{CR}(\gamma)/P_{CR}(180°)$
0°	276	262	340	293	0.14
45°	280	240	255	258	0.12
90°	315	350	310	325	0.16
120°	405	417	390	404	0.20
150°	592	640	675	636	0.31
180°	2280	1860	2010	2050	1.00

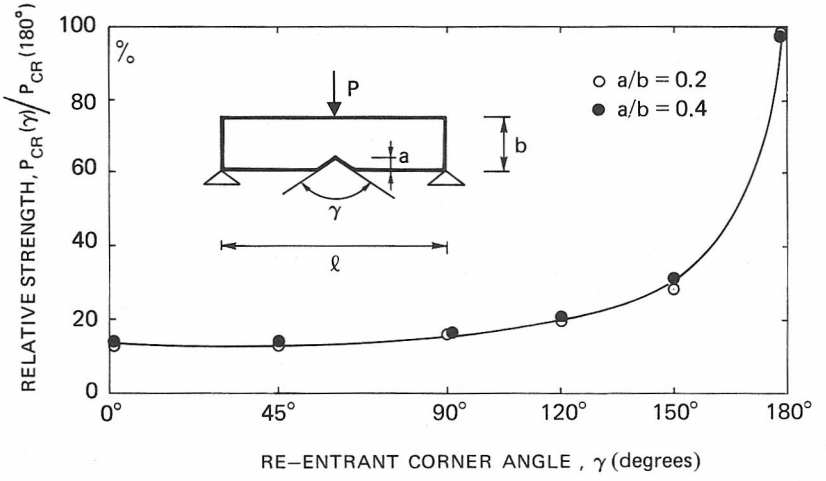

Fig. 6. Relative strength vs re-entrant corner angle.

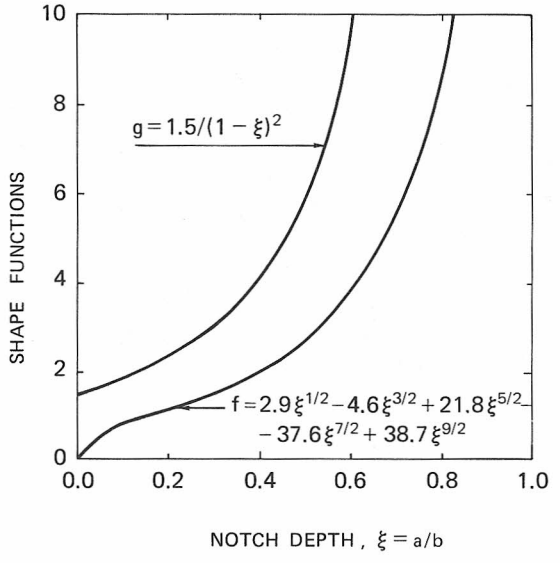

Fig. 7. Shape-functions for 0° and 180° re-entrant corner angle.

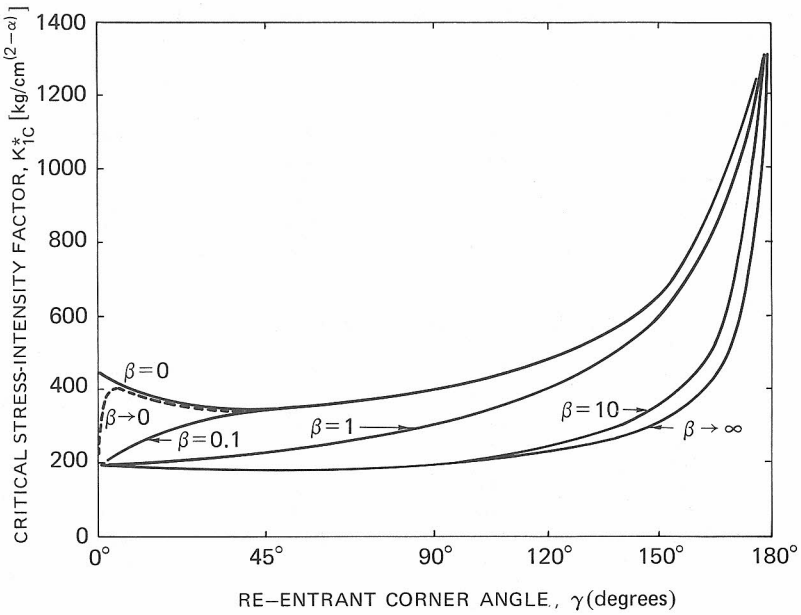

Fig. 8. Critical stress intensity factor vs re-entrant corner angle.

linear variation may be approximated as:

$$C(\gamma) \simeq \frac{1}{2}\left[1+\left(\frac{\gamma}{\pi}\right)^{\beta}\right], \tag{25}$$

where β is an unknown exponent. A more precise form of function f^* may be expressed as a non-linear combination of LEFM function f and ultimate strength function g:

$$K_1^* = \frac{Pl}{tb^{(2-\alpha)}}\left\{f\left(\frac{a}{b}\right)+\left(\frac{\gamma}{\pi}\right)^{\beta}\left[g\left(\frac{a}{b}\right)-f\left(\frac{a}{b}\right)\right]\right\}. \tag{26}$$

The critical values of the generalized stress-intensity factor are computed according to eq. (26), using the experimental average values of failure load $P_{CR}(\gamma)$ given in the Tables 1 and 2 and the singularity powers $\alpha(\gamma)$ represented in Fig. 3. The influence of the exponent β is explored over a wide range of values, from zero to infinity. The notch toughness K^*_{1C} appears very sensible to the variation in corner angle γ and exponent β, whereas the values related to different relative notch depths a/b (γ and β being the same) are very close. The computed critical stress-intensity factors are represented in Fig. 8 against the re-entrant corner angle γ and by varying the exponent β. Each one of the five curves β = constant represents the transition from classical fracture toughness K_{1C} to ultimate tensile strength σ_u. Obviously, the physical dimensions of K^*_{1C} vary by varying angle γ. They are kg/cm$^{[2-\alpha(\gamma)]}$, where $\alpha(\gamma)$ is the function represented in Fig. 3. We observe that, for $\beta \to 0^+$, the convergence of function $K^*_{1C}(\gamma, \beta)$ is non-uniform at $\gamma = 0°$, and that K^*_{1C} can appear increasing or decreasing in dependence on material and units of measure.

For $\beta \to 0^+$ we have toughnesses K^*_{1C} which, on the average, are twice those obtained for $\beta \to \infty$. Unfortunately, for none of the β values the two K^*_{1C} values obtained for $a/b = 0.2$ and 0.4, respectively, are particularly closer than in the other cases. Numbering the corner angles from 1 to 6 and indicating with ΔK_i the difference between ith K^*_{1C} value for $a/b = 0.2$ and that for $a/b = 0.4$, the following linear and quadratic deviations are computed:

$$L = \frac{1}{6}\sum_{i=1}^{6} |\Delta K_i/K_i|, \tag{27}$$

$$Q = \left[\frac{1}{6}\sum_{i=1}^{6} (\Delta K_i/K_i)^2\right]^{1/2}. \tag{28}$$

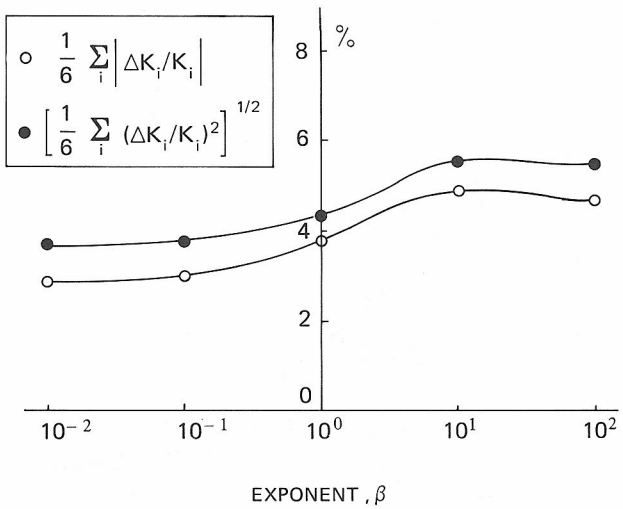

Fig. 9. Linear and quadratic deviations for the generalized fracture toughness.

They are plotted in Fig. 9. It results that L and Q are always very small, for any value of exponent β. They approximately range between 3 and 5%. The extreme cases $\gamma = 0°$ and $\gamma = 180°$ really do not contribute to the variation of L and Q with β, since the K^*_{1C} values do not depend on exponent β in those cases, see eq. (26). From Fig. 9 it follows that the most uniform results, $a/b = 0.2$ vs $a/b = 0.4$, are obtained for $\beta \to 0^+$. On the other hand, even for $\beta \to \infty$ the results of the different crack depths appear relatively close, so that it is nearly impossible to determine which of the curves in Fig. 8 is the true material characterization. Such an indetermination is due to the very similar aspect of functions f and g in Fig. 7.

4. ATTENUATION OF THE SCALE EFFECTS

If both the members of eq. (26) are divided by the product $\sigma_u b^\alpha$ and considered at the failure condition, we obtain:

$$\frac{K^*_{1C}}{\sigma_u b^\alpha} = \frac{P_{CR} l}{t b^2 \sigma_u} f^*\left(\frac{a}{b}, \gamma\right). \tag{29}$$

Equation (29) can be rearranged in the following form:

$$\frac{P_{CR} l}{t b^2 \sigma_u} = \frac{s}{f^*(a/b, \gamma)}, \tag{30}$$

where the non-dimensional number:

$$s = \frac{K^*_{1C}}{\sigma_u b^\alpha}, \tag{31}$$

is a measure of the brittleness of the system, being a function of material properties (ultimate tensile strength σ_u and generalized fracture toughness K^*_{1C}) and structural size scale b[8, 9].

At the same time, the dimensionless load of ultimate strength at the ligament is:

$$\frac{P_{CR} l}{t b^2 \sigma_u} = \frac{1}{g(a/b)}. \tag{32}$$

Whereas the condition of stress-intensity collapse, eq. (30), represents a family of curves in the plane $P_{CR} l/t b^2 \sigma_u$ vs a/b by varying the brittleness number s, the condition of ultimate strength collapse, eq. (32), represents a unique curve in the same plane.

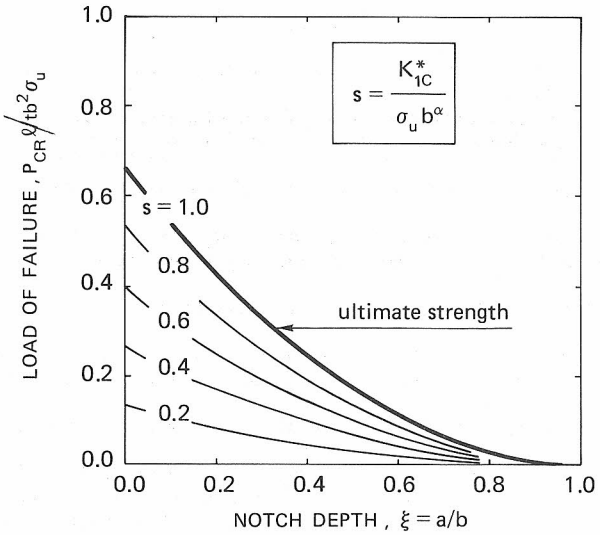

Fig. 10. Load of failure versus notch depth by varying the brittleness number s ($\beta = 0$).

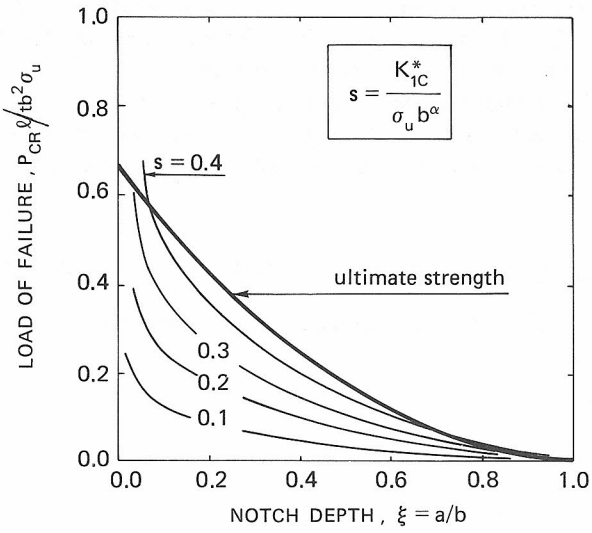

Fig. 11. Load of failure vs notch depth by varying the brittleness number s ($\beta \to \infty$ or $\gamma = 0$).

For example, if $0 < \gamma < \pi$ and $\beta = 0$ the family of curves of stress-intensity collapse is represented in Fig. 10. It is always the same family for every angle $\gamma \neq 0, \pi$. When $\beta \to \infty$ the family of curves changes as shown in Fig. 11.

If $0 < \beta < \infty$ and $\gamma = 0$ the family of curves is that shown in Fig. 11, whereas for $\gamma = \pi$ the family of curves collapses into a unique ultimate strength curve, being in this latter case $K^*_{1C} = \sigma_u, \alpha = 0$ and then $s \equiv 1$.

More generally, if $0 < \gamma < \pi$ and $0 < \beta < \infty$, for each pair of values γ and β there is a different family of stress-intensity collapse curves. In any case (except for $\gamma = \pi$) there is an upper bound to number s above which the stress-intensity collapse is obscured by the ultimate strength collapse. In Fig. 10 this limit is $s_0 = 1.0$, whereas in Fig. 11 it is $s_0 = 0.5$. In all the remaining cases, for any γ and β values, the limit s_0 is included between 0.5 and 1.0.

It is evident that an attenuation of the scale effects occurs by decreasing the size scale b and/or increasing the re-entrant corner angle γ. For very small sizes ($s \to \infty$) and/or when the re-entrant corner angle is exactly flat ($\gamma = \pi$) any scale effect disappears.

Acknowledgement—The author gratefully acknowledges the financial support of M.P.I. and C.N.R.

REFERENCES

[1] M. L. Williams, Stress singularities resulting from various boundary conditions in angular corners of plates in extension. *J. appl. Mech.* **19,** 526–528 (1952).
[2] G. R. Irwin, Analysis of stresses and strains near the end of a crack traversing a plate. *J. appl. Mech.* **24,** 361–364 (1957).
[3] R. H. Leicester, Effect of size on the strength of structures. CSIRO Forest Products Laboratory, Division of Building Research, Paper No. 71 (1973).
[4] P. F. Walsh, Linear fracture mechanics solutions for zero and right angle notches. CSIRO Division of Building Research, Paper No. 2 (1974).
[5] P. F. Walsh, Crack initiation in plain concrete. *Mag. Concrete Res.* **28,** 37–41 (1976).
[6] G. B. Sinclair and M. Kondo, On the stress concentration at sharp re-entrant corners in plates. *Int. J. Mechanical Sci.* **26,** 477–487 (1984).
[7] W. C. Carpenter, Mode I and mode II stress intensities for plates with cracks of finite opening. *Int. J. Fracture* **26,** 201–214 (1984).
[8] A. Carpinteri, Notch sensitivity in fracture testing of aggregative materials. *Engng Fracture Mech.* **16,** 467–481 (1982).
[9] A. Carpinteri, C. Marega and A. Savadori, Ductile–brittle transition by varying structural size. *Engng Fracture Mech.* **21,** 263–271 (1985).
[10] A. Carpinteri, Plastic flow collapse versus separation collapse in elastic–plastic strain-hardening structures. *Mater. Struc.* **16,** 85–96 (1983).
[11] Standard method of test for plane strain fracture toughness of metallic materials, E 399-74, ASTM.
[12] G. Di Leonardo, Fracture toughness characterization of materials under multiaxial loading. *Int. J. Fracture* **15,** 537–552 (1979).

(*Received* 19 *March* 1986)